

# Low-Bandgap Mixed Tin–Lead Perovskite Solar Cells

Jingwei Zhu, Cong Chen and Dewei Zhao \*

Engineering Research Center of Alternative Energy Materials & Devices, College of Materials Science and Engineering, Ministry of Education, Sichuan University, Chengdu 610065, China; zjw03jiayou@163.com (J.Z.); chen.cong@scu.edu.cn (C.C.)

\* Correspondence: dewei.zhao@scu.edu.cn

**Abstract:** Low-bandgap mixed tin (Sn)–lead (Pb) perovskite solar cells have been extensively investigated in the past few years due to their great potential in high-performance perovskite/perovskite tandem solar cells. From this perspective, we briefly summarize the mechanism of understanding of additives and the advances in the efficiency and stability of such low-bandgap Sn-Pb perovskite materials and solar cells in terms of various effective strategies for suppressing the defects and oxidation of  $\text{Sn}^{2+}$ , regulating crystallization growth, etc. We then provide a perspective regarding the achievement of high-quality, low-bandgap Sn-Pb perovskites and highly efficient solar cells.

**Keywords:** low-bandgap perovskites; perovskite solar cells; tandem solar cells; mixed tin–lead

Organometallic halide perovskites have been considered as promising optoelectronic materials owing to their unique advantages including a high absorption coefficient, long carrier diffusion length and low-cost solution processability [1–3]. The certified power conversion efficiency (PCE) of single-junction perovskite solar cells (PSCs) has been increased to 25.7% in just a decade, approaching the Shockley–Queisser (S-Q) limits [4]. Perovskite/perovskite (all-perovskite) tandem solar cells (TSCs), consisting of wide-bandgap ( $E_g \sim 1.7\text{--}1.9$  eV) top subcells and low-bandgap ( $E_g \sim 1.2\text{--}1.3$  eV) bottom subcells, have the potential to break the S-Q limits [5–8]. The PCEs of wide- $E_g$  top cells have been significantly improved through unremitting efforts. However, it is still challenging to fabricate high-performance, low- $E_g$  mixed tin–lead (Sn-Pb) bottom cells due to the uncontrollable perovskite film quality and unsatisfactory device stability.

To date, the development of low- $E_g$  mixed Sn-Pb PSCs still lags behind that of their Pb counterparts, irrespective of their advantages that enable ideal bandgaps for yielding higher PCEs according to S-Q predictions. The aforementioned dilemma can be mainly ascribed to the following issues: (1) inferior film quality with uncontrollable morphology and high density of trap states caused by heterogeneous nucleation and accelerated crystallization; (2) numerous Sn vacancies caused by self-p-doping due to the easy oxidation of  $\text{Sn}^{2+}$  to  $\text{Sn}^{4+}$  [9]. These further shorten carrier lifetimes and mobility and increase background hole concentrations and serious non-radiative recombination, thus leading to the unsatisfactory efficiency and stability of Sn-Pb PSCs. Therefore, high-quality Sn-Pb perovskite film is the prerequisite of efficient Sn-Pb devices.

To address the abovementioned issues, researchers have devoted great efforts to improving the quality of mixed Sn-Pb perovskite film and fabricating high-performance, low- $E_g$  devices. In 2014, Hayase et al. synthesized low- $E_g$  PSCs with a regular structure by employing alloyed  $\text{MASn}_{0.5}\text{Pb}_{0.5}\text{I}_3$  as the absorber and mesoporous  $\text{TiO}_2$  as the electron transport layer and achieved a PCE of 4.18% with an open-circuit voltage ( $V_{OC}$ ) of 0.42 V, a short-circuit current ( $J_{SC}$ ) of  $20.04 \text{ mA cm}^{-2}$  and a fill factor (FF) of 50% [10]. They found that  $\text{MASn}_{0.5}\text{Pb}_{0.5}\text{I}_3$  perovskite can absorb near-infrared light with the absorption onset at 1060 nm. In the same year, Zuo et al. demonstrated that optimizing the synthetic conditions can help to improve the film quality of  $\text{MAPb}_{0.85}\text{Sn}_{0.15}\text{I}_3$  perovskites on ITO/PEDOT:PSS substrates (Figure 1a), leading to efficient inverted Sn-Pb PSCs with a PCE exceeding 10%



**Citation:** Zhu, J.; Chen, C.; Zhao, D. Low-Bandgap Mixed Tin–Lead Perovskite Solar Cells. *Solar* **2022**, *2*, 334–340. <https://doi.org/10.3390/solar2030019>

Academic Editor: Marko Topic

Received: 8 May 2022

Accepted: 22 June 2022

Published: 1 July 2022

**Publisher's Note:** MDPI stays neutral with regard to jurisdictional claims in published maps and institutional affiliations.



**Copyright:** © 2022 by the authors. Licensee MDPI, Basel, Switzerland. This article is an open access article distributed under the terms and conditions of the Creative Commons Attribution (CC BY) license (<https://creativecommons.org/licenses/by/4.0/>).

( $V_{OC} = 0.77$  V,  $J_{SC} = 19.5$  mA cm<sup>-2</sup>, FF = 67%) [11]. In 2016, Yan's group reported a novel mixture strategy of combining individual MAPbI<sub>3</sub> and FASnI<sub>3</sub> precursors to prepare high-quality Sn-Pb perovskite film with uniform grain sizes and smooth surfaces. By adjusting the composition of Sn, they achieved high-quality perovskite film (the corresponding carrier lifetime was 6.7 ns) and efficient PSCs with PCEs over 15.08% based on the optimal composition of (FASnI<sub>3</sub>)<sub>0.6</sub>(MAPbI<sub>3</sub>)<sub>0.4</sub>, and the optimized PSCs also exhibited the obviously improved  $V_{OC}$  (0.795 V),  $J_{SC}$  (26.86 mA cm<sup>-2</sup>), and FF (70.6%) [12]. In 2017, Zhao et al. increased the thickness of a (FASnI<sub>3</sub>)<sub>0.6</sub>(MAPbI<sub>3</sub>)<sub>0.4</sub> absorber layer from 400 to 620 nm by regulating the perovskite growth process. The final perovskite film displayed enlarged grains and a prolonged carrier lifetime (~250 ns), enabling efficient Sn-Pb ( $E_g \sim 1.25$  eV) PSCs with the best PCE of over 17.6% (certified 17.01%), with a  $V_{OC}$  of 0.853 V, a  $J_{SC}$  of 28.5 mA cm<sup>-2</sup>, and a FF of 72.5% [13]. After that, they further reported low- $E_g$  PSCs with 18.1% and ~19% efficiency (other photovoltaic parameters are summarized in Table 1) via chlorine and bromine incorporation, respectively, to increase the grain size, reduce electronic disorder, passivate the grain boundaries, and slightly regulate the bandgap of (FASnI<sub>3</sub>)<sub>0.6</sub>(MAPbI<sub>3</sub>)<sub>0.4</sub> perovskite films [14,15]. Meanwhile, perovskite films with chlorine and bromine incorporation exhibited the longer photocurrent decay time of 292  $\mu$ s and the longer mean carrier lifetime of 228 ns, respectively.

In 2019, Zhu et al. demonstrated that guanidinium thiocyanate (GuaSCN) additive can effectively passivate defect states, suppress the formation of excessive Sn vacancies, and reduce the oxidation of Sn<sup>2+</sup> in (FASnI<sub>3</sub>)<sub>0.6</sub>(MAPbI<sub>3</sub>)<sub>0.4</sub> film without changing the bandgap of perovskite, leading to low- $E_g$  PSCs with 20.5% efficiency ( $V_{OC} = 0.834$  V,  $J_{SC} = 30.4$  mA cm<sup>-2</sup>, FF = 80.8%) due to the prolonged carrier lifetime (1232 ns) and diffusion length (2.5  $\mu$ m) [16]. Tan et al. reported a comproportionating strategy via adding a small amount of Sn powders to suppress the oxidation of Sn<sup>2+</sup> in the precursor and consequently enhance the carrier diffusion length in low- $E_g$  Sn-Pb perovskite films [17]. This strategy significantly reduced the Sn vacancies inside the grains and increased the carrier diffusion length to 3  $\mu$ m in the final films, enabling efficient low- $E_g$  PSCs with the best PCE of 21.1%, together with a  $V_{OC}$  of 0.831 V, a  $J_{SC}$  of 31.4 mA cm<sup>-2</sup>, and a FF of 80.8%, which were obviously higher than the corresponding parameters of 18.3%, 0.811 V, 29.1 mA cm<sup>-2</sup>, and 77.7% for the control MA<sub>0.3</sub>FA<sub>0.7</sub>Pb<sub>0.5</sub>Sn<sub>0.5</sub>I<sub>3</sub> PSCs, respectively. In 2020, they employed surface-anchoring zwitterionic molecules, i.e., formamidine sulfonic acid (FSA), as additives to further inhibit Sn<sup>2+</sup> oxidation and passivate defects on the grain surfaces, therefore prolonging the charge-carrier lifetime to 43 ns in mixed Sn-Pb perovskite films without affecting the bandgap, boosting the PCE from 19.4% for the control device to 21.7% for the FSA-modified low- $E_g$  PSCs. In addition, the solar cell exhibited a certified efficiency of 20.74% with a  $V_{OC}$  of 0.841 V, a  $J_{SC}$  of 30.6 mA cm<sup>-2</sup>, and a FF of 80.6% [18]. It is easy to determine that additives play vital roles in achieving high-quality Sn-Pb perovskite films and therefore high-performance devices. However, the underlying mechanisms are not well understood yet, especially for the most commonly used SnF<sub>2</sub> additives in high-quality Sn-Pb perovskite films and efficient low- $E_g$  devices.

In 2021, Zhao et al. systematically explored the effects of SnF<sub>2</sub> additives on low- $E_g$  mixed Sn-Pb perovskite films and solar cells [19]. They found that the surface morphology of Sn-Pb perovskite films with SnF<sub>2</sub> additives exhibited regular linear stripes, which was obviously different to the "clean morphology" of the control sample without SnF<sub>2</sub> (Figure 1b). Moreover, the SnF<sub>2</sub>-incorporated Sn-Pb perovskite exhibited a highly uniform and ordered mode, as shown in the cross-sectional SEM image (Figure 1c). They attributed the formation of the "domain morphology" to crystal topological growth caused by the doping of SnF<sub>2</sub> in the perovskite precursor solution (Figure 1d). The bandgap of the perovskite did not change after employing SnF<sub>2</sub>. In addition, the carrier lifetime of 5% SnF<sub>2</sub>-doped perovskite film was 98 ns, which was significantly higher than 20 ns, which was determined for the SnF<sub>2</sub>-free perovskite sample. Interestingly, the F<sup>-</sup> ions accumulated preferentially at the PEDOT:PSS/perovskite interface, and the distribution of F<sup>-</sup> increased monotonically with the increased SnF<sub>2</sub> concentration (Figure 1e). However, excessive

$\text{SnF}_2$  additive hindered the hole transport process at the PEDOT:PSS/perovskite interface and led to a significant difference in EQE values from 350 to 500 nm for various devices (Figure 1f). Finally, they concluded that the  $\text{SnF}_2$  additive can promote the topological growth of perovskite grains and inhibit the oxidation of  $\text{Sn}^{2+}$  and the formation of Sn vacancies, enabling efficient Sn-Pb PSCs with a promising PCE of 20.27% ( $V_{\text{OC}} = 0.834$  V,  $J_{\text{SC}} = 30.4$   $\text{mA cm}^{-2}$ , and  $\text{FF} = 80.8\%$ ), which was much higher than the 12.21% efficiency obtained for  $\text{SnF}_2$ -free PSCs.

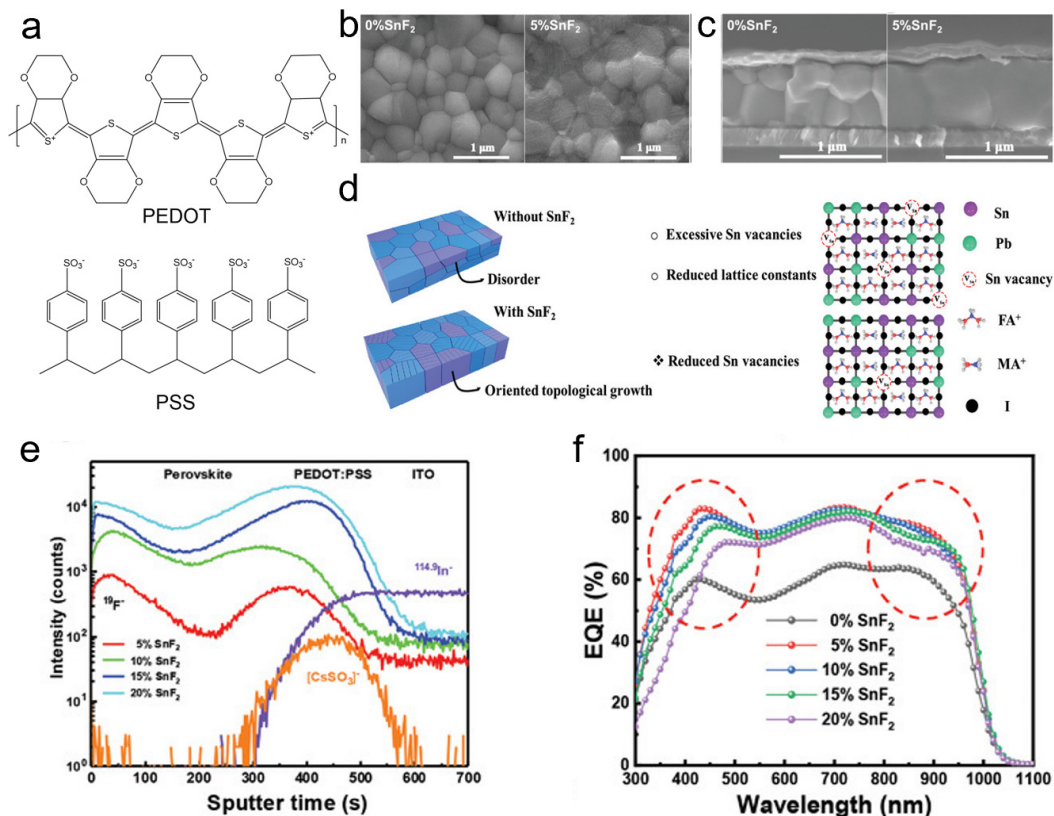


**Figure 1.** (a) The chemical structures of PEDOT:PSS. (b) Top-view and (c) cross-sectional SEM images of  $(\text{FASnI}_3)_{0.6}(\text{MAPbI}_3)_{0.4}$  films with 0% and 5%  $\text{SnF}_2$ . (d) Schematic illustration of the influence of  $\text{SnF}_2$  on  $(\text{FASnI}_3)_{0.6}(\text{MAPbI}_3)_{0.4}$  perovskite growth. (e) ToF-SIMS depth profile of ITO/PEDOT:PSS/ $(\text{FASnI}_3)_{0.6}(\text{MAPbI}_3)_{0.4}$  films with different  $\text{SnF}_2$  concentrations. (f) EQE spectra of devices with different  $\text{SnF}_2$  concentrations. Reprinted/adapted with permission from Ref. [19]. Copyright 2021, Wiley-VCH.

Recently, Tan et al. investigated the passivation capability of three aromatic ammonium cations, phenethylammonium (PEA), phenylammonium (PA), and 4-trifluoromethylphenylammonium (CF3-PA), on low- $E_g$  mixed Sn-Pb perovskite surfaces (Figure 2a) [20]. The density functional theory (DFT) (Figure 2b,c) and ab initio molecular dynamics simulations (Figure 2d) indicated that CF3-PA had the strongest potential to passivate the acceptor-type defects in the perovskite grain surface (Figure 2e). As expected, the perovskite film with the CF3-PA passivating agent displayed the longest carrier lifetime of 966 ns (Figure 2f) and carrier diffusion length of 5.4  $\mu\text{m}$  (Figure 2g). Meanwhile, their results suggested that the incorporation of CF3-PA did not change the bandgap of Sn-Pb perovskites. With the optimal film thickness of 1.2  $\mu\text{m}$ , CF3-PA-treated Sn-Pb PSCs yielded a PCE of 22.2% (a  $V_{\text{OC}}$  of 0.841 V, a  $J_{\text{SC}}$  of 33.0  $\text{mA cm}^{-2}$ , and a  $\text{FF}$  of 80%) (Figure 2h). Furthermore, CF3-PA-passivated all-perovskite TSCs obtained a certified efficiency of 26.4% with a  $V_{\text{OC}}$  of 2.048 V, a  $J_{\text{SC}}$  of 16.54  $\text{mA cm}^{-2}$ , and a  $\text{FF}$  of 77.9%, which surpassed that of the best-performing single-junction PSCs for the first time.

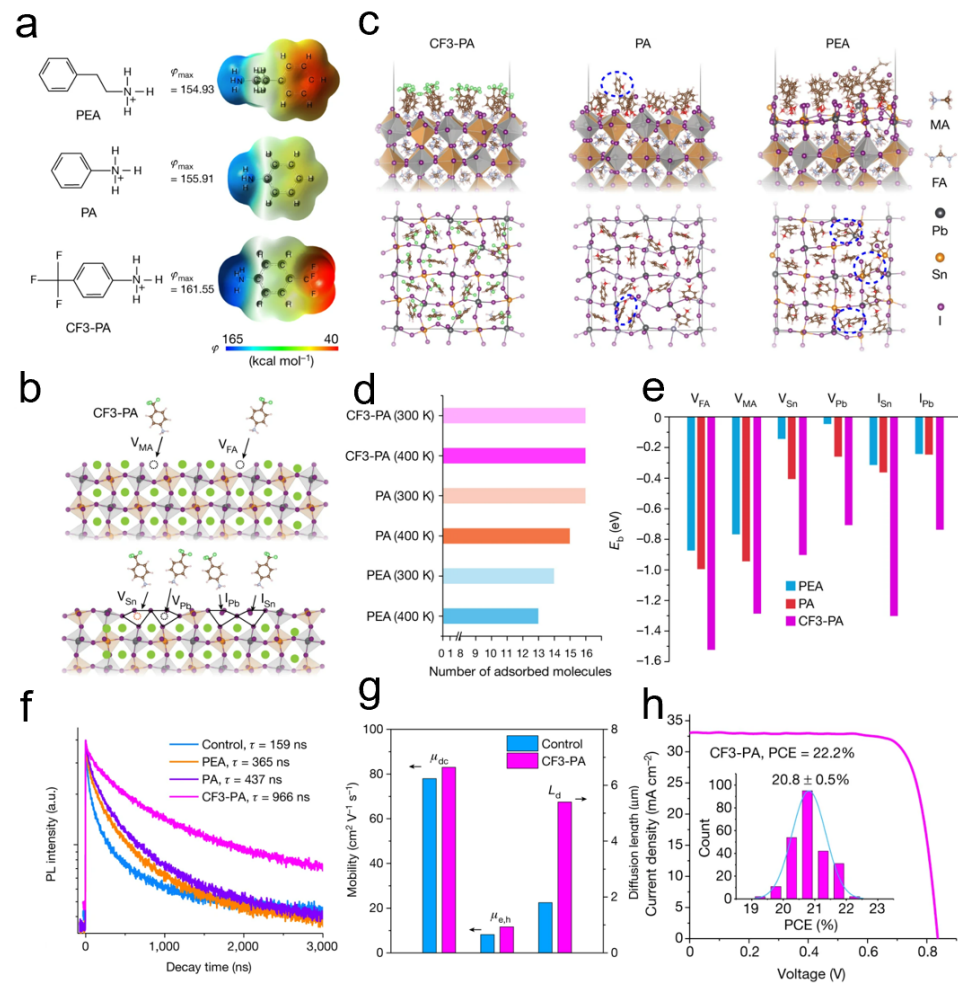


**Figure 2.** (a) The molecular structures of three passivators (PEA, PA, and CF3-PA). (b) Schematic diagram of the interaction between ammonium cations with the acceptor-like defects. (c) Ab initio molecular dynamics snapshots and top views of the CF3-PA-, PA-, and PEA-adsorbed perovskite surfaces at a temperature of 400 K. (d) The number of adsorbed molecules for CF3-PA, PA, and PEA at temperatures of 300 and 400 K. (e) The binding energy ( $E_b$ ) between passivators and various acceptor-like defects. (f) Time-resolved PL spectra of the control, PEA, PA, and CF3-PA perovskite films. (g) Mobilities and diffusion lengths of the CF3-PA and control Pb-Sn perovskite films. (h)  $J-V$  curves of the best CF3-PA device (with 1.2  $\mu\text{m}$  thick absorber). The inset shows the PCE distribution of 237 CF3-PA devices, showing an average PCE of  $20.8 \pm 0.5\%$ . Reprinted/adapted with permission from Ref. [20]. Copyright 2022, Nature Publishing Group.

In addition to the efficiency enhancement of low- $E_g$  Sn-Pb PSCs, the unsatisfactory stability caused by volatile  $\text{MA}^+$  cations is also an urgent issue that needs to be addressed. Li et al. successfully decreased the MA proportion to 10% and prepared high-quality  $\text{FA}_{0.85}\text{MA}_{0.1}\text{Cs}_{0.05}\text{Sn}_{0.5}\text{Pb}_{0.5}\text{I}_3$  perovskite film using two-step bilayer interdiffusion growth technology. They further employed pyrrolidinium thiocyanate (PySCN) to passivate the defects at grain boundaries and on the film surface. The resulting mixed Sn-Pb PSCs yielded the best PCE of 20.4% with a  $V_{OC}$  of 0.865 V, a  $J_{SC}$  of  $29.81 \text{ mA cm}^{-2}$ , and a FF of 79.1%, while the control device could only obtain about 19% PCE output. More importantly, the optimized PSCs exhibited excellent stability upon light and heat stress, and the encapsulated devices retained 92% of the initial PCE under continuous illumination ( $100 \text{ mW cm}^{-2}$ ) for over 450 h [21]. More recently, Zhou et al. effectively regulated the energy disorder of mixed Sn-Pb perovskite films and restrained the oxidation of  $\text{Sn}^{2+}$  by the additives of  $\text{SnF}_2$  and 1-bromo-4-(methylsulfinyl) benzene (BBMS). Moreover, compared to the control sample,

the deeper valence band of BBMS-added perovskite film could boost the extraction of holes from perovskite to PEDOT:PSS. As a result, compared to the PCE of 18.97% ( $V_{OC} = 0.824$  V,  $J_{SC} = 30.5$  mA cm<sup>-2</sup>, FF = 75.5%) for the control PSCs, the SnF<sub>2</sub>-BBMS-tailored Sn-Pb PSCs exhibited the best PCE of up to 22.03% ( $V_{OC} = 0.849$  V,  $J_{SC} = 32.2$  mA cm<sup>-2</sup>, FF = 80.6%) with superior thermal stability, retaining 98% initial efficiency after continuous heating at 60 °C for over 110 days [22]. From the above analysis, we can see that employing additives into perovskite films can effectively improve the stability of low- $E_g$  mixed Sn-Pb PSCs, cross-checking the reports in other bandgap PSCs and related fields [23–28]. However, low- $E_g$  mixed Sn-Pb PSCs show inferior long-term stability to pure Pb analogues, encouraging more efforts devoted to film quality improvement strategies and degradation mechanisms.

**Table 1.** Summary of the photovoltaic parameters of low- $E_g$  Sn-Pb PSCs with the best PCE.

Device Structure	$J_{SC}$ (mA cm <sup>-2</sup> )	$V_{OC}$ (V)	FF (%)	PCE (%)	Ref.
FTO/c-TiO <sub>2</sub> /CH <sub>3</sub> NH <sub>3</sub> Sn <sub>0.5</sub> Pb <sub>0.5</sub> I <sub>3</sub> /P3HT/Ag	20.04	0.42	50.0	4.18	[10]
ITO/PEDOT:PSS/MASn <sub>0.15</sub> Pb <sub>0.85</sub> I <sub>3</sub> /PCBM/Bis-salt/Ag	19.5	0.77	67.0	10.1	[11]
ITO/PEDOT:PSS/(FASnI <sub>3</sub> ) <sub>0.6</sub> (MAPbI <sub>3</sub> ) <sub>0.4</sub> /C60/BCP/Ag	26.86	0.795	70.6	15.08	[12]
ITO/PEDOT:PSS/(FASnI <sub>3</sub> ) <sub>0.6</sub> (MAPbI <sub>3</sub> ) <sub>0.4</sub> /C60/BCP/Ag	28.5	0.853	72.5	17.6	[13]
ITO/PEDOT:PSS/(FASnI <sub>3</sub> ) <sub>0.6</sub> (MAPbI <sub>3</sub> ) <sub>0.4</sub> :Cl/C60/BCP/Ag	29.0	0.841	74.4	18.1	[14]
ITO/PEDOT:PSS/(FASnI <sub>3</sub> ) <sub>0.6</sub> (MAPbI <sub>3</sub> ) <sub>0.4</sub> :Br/C60/BCP/Ag	28.72	0.888	74.6	19.03	[15]
ITO/PEDOT:PSS/(FASnI <sub>3</sub> ) <sub>0.6</sub> (MAPbI <sub>3</sub> ) <sub>0.4</sub> :GuaSCN/C60/BCP/Ag	30.4	0.834	80.8	20.5	[16]
ITO/PEDOT:PSS/FA <sub>0.7</sub> MA <sub>0.3</sub> Pb <sub>0.5</sub> Sn <sub>0.5</sub> I <sub>3</sub> :Sn powder/C60/BCP/Cu	31.4	0.831	80.8	21.1	[17]
ITO/PEDOT:PSS/FA <sub>0.7</sub> MA <sub>0.3</sub> Pb <sub>0.5</sub> Sn <sub>0.5</sub> I <sub>3</sub> :FSA/C60/BCP/Cu	31.6	0.850	80.8	21.7	[18]
ITO/PEDOT:PSS/(FASnI <sub>3</sub> ) <sub>0.6</sub> (MAPbI <sub>3</sub> ) <sub>0.4</sub> :SnF <sub>2</sub> /C60/BCP/Ag	30.6	0.834	79.4	20.27	[19]
ITO/PEDOT:PSS/FA <sub>0.7</sub> MA <sub>0.3</sub> Pb <sub>0.5</sub> Sn <sub>0.5</sub> I <sub>3</sub> :CF <sub>3</sub> -PA/C60/BCP/Cu	33.0	0.841	80.0	22.2	[20]
ITO/PEDOT:PSS/FA <sub>0.7</sub> MA <sub>0.3</sub> Pb <sub>0.5</sub> Sn <sub>0.5</sub> I <sub>3</sub> :PySCN/C60/BCP/Ag	29.81	0.865	79.1	20.4	[21]
ITO/PEDOT:PSS/(FASnI <sub>3</sub> ) <sub>0.6</sub> (MAPbI <sub>3</sub> ) <sub>0.4</sub> :BBMS/C60/BCP/Ag	32.2	0.849	80.6	22.03	[22]
FTO/PEDOT:PSS/Cs <sub>0.1</sub> FA <sub>0.6</sub> MA <sub>0.3</sub> Pb <sub>0.5</sub> Sn <sub>0.5</sub> I <sub>3</sub> :GlyHCl/EDAI <sub>2</sub> /C60/BCP/Ag	32.5	0.89	82	23.6	[29]
FTO/2PACz/MPA/Cs <sub>0.025</sub> FA <sub>0.475</sub> MA <sub>0.5</sub> Sn <sub>0.5</sub> Pb <sub>0.5</sub> I <sub>2.925</sub> Br <sub>0.075</sub> /C60/PCBM/BCP/Ag	32.77	0.88	80	23.3	[30]

Thus far, the PCEs of the state-of-the-art, low- $E_g$  mixed Sn-Pb PSCs have exceeded 23.6% [29], but these values are still far from their theoretical efficiency limits. Further development and efforts toward the creation of efficient low- $E_g$  mixed Sn-Pb PSCs should be focused on the following aspects: (1) systematically exploring the crystallization mechanism of Sn-Pb perovskites. The fast and uncontrollable crystallization process is the fundamental reason for unsatisfactory Sn-contained perovskite film quality and device performance [9]. Thus, it is imperative to propose effective strategies for developing an advanced film fabrication technique. (2) Suppressing the oxidation of Sn<sup>2+</sup> to Sn<sup>4+</sup> which leads to the heavy self-p-doping of mixed Sn-Pb perovskites to eliminate defects, as well as increasing the carrier lifetimes and diffusion lengths. Effective reductive agents and passivators are highly desired to reduce defects such as Sn vacancies and Sn<sup>4+</sup>. A mechanism for Sn<sup>4+</sup> detection is also urgently needed [31]. (3) Optimizing the compositions (especially reducing the MA proportion) and thicknesses of perovskite films to strengthen halide structures and bandgaps of Sn-Pb PSCs [13,20,21]. (4) Developing novel charge-selective materials for efficient and stable low- $E_g$  mixed Sn-Pb PSCs [30]. With all these efforts, low- $E_g$  mixed Sn-Pb perovskites will demonstrate considerable promise in diverse optoelectronic applications.

**Author Contributions:** Conceptualization, D.Z. and J.Z.; validation, J.Z., C.C. and D.Z.; writing—original draft preparation, J.Z.; writing—review and editing, J.Z., C.C. and D.Z.; visualization, D.Z.; supervision, D.Z.; funding acquisition, D.Z. All authors have read and agreed to the published version of the manuscript.

**Funding:** This work was financially supported by the Fundamental Research Funds for the Central Universities (nos. YJ201955 and YJ2021157), the Science and Technology Program of Sichuan Province (no. 2020JDJQ0030) and the Engineering Featured Team Fund of Sichuan University (2020SCUNG102).

**Institutional Review Board Statement:** Not applicable.

**Informed Consent Statement:** Not applicable.

**Data Availability Statement:** Not applicable.

**Conflicts of Interest:** The authors declare no conflict of interest.

## References

1. Jeong, M.; Choi, I.W.; Go, E.M.; Cho, Y.; Kim, M.; Lee, B.; Jeong, S.; Jo, Y.; Choi, H.W.; Lee, J.; et al. Stable perovskite solar cells with efficiency exceeding 24.8% and 0.3-V voltage loss. *Science* **2020**, *369*, 1615–1620. [PubMed]
2. He, Y.; Petryk, M.; Liu, Z.; Chica, D.G.; Hadar, I.; Leak, C.; Ke, W.; Spanopoulos, I.; Lin, W.; Chung, D.Y.; et al. CsPbBr<sub>3</sub> perovskite detectors with 1.4% energy resolution for high-energy  $\gamma$ -rays. *Nat. Photonics* **2021**, *15*, 36–42. [CrossRef]
3. Schulz, P.; Cahen, D.; Kahn, A. Halide perovskites: Is it all about the interfaces? *Chem. Rev.* **2019**, *119*, 3349–3417. [CrossRef] [PubMed]
4. Best Research-Cell Efficiency Chart. Available online: <https://www.nrel.gov/pv/cell-efficiency.html> (accessed on 7 May 2022).
5. Eperon, G.E.; Leijtens, T.; Bush, K.A.; Prasanna, R.; Green, T.; Wang, J.T.-W.; McMeekin, D.P.; Volonakis, G.; Milot, R.L.; May, R.; et al. Perovskite-perovskite tandem photovoltaics with optimized band gaps. *Science* **2016**, *354*, 861–865. [CrossRef]
6. Zhao, D.; Ding, L. All-perovskite tandem structures shed light on thin-film photovoltaics. *Sci. Bull.* **2020**, *65*, 1144–1146. [CrossRef]
7. Fang, Z.; Zeng, Q.; Zuo, C.; Zhang, L.; Xiao, H.; Cheng, M.; Hao, F.; Bao, Q.; Zhang, L.; Yuan, Y.; et al. Perovskite-based tandem solar cells. *Sci. Bull.* **2021**, *66*, 621–636. [CrossRef]
8. He, R.; Ren, S.; Chen, C.; Yi, Z.; Luo, Y.; Lai, H.; Wang, W.; Zeng, G.; Hao, X.; Wang, Y.; et al. Wide-bandgap organic-inorganic hybrid and all-inorganic perovskite solar cells and their application in all-perovskite tandem solar cells. *Energy Environ. Sci.* **2021**, *14*, 5723–5759. [CrossRef]
9. Wang, C.; Song, Z.; Li, C.; Zhao, D.; Yan, Y. Low-bandgap mixed tin-lead perovskites and their applications in all-perovskite tandem solar cells. *Adv. Funct. Mater.* **2019**, *29*, 1808801. [CrossRef]
10. Ogomi, Y.; Morita, A.; Tsukamoto, S.; Saitho, T.; Fujikawa, N.; Shen, Q.; Toyoda, T.; Yoshino, K.; Pandey, S.S.; Ma, T.; et al. CH<sub>3</sub>NH<sub>3</sub>Sn<sub>x</sub>Pb<sub>(1-x)</sub>I<sub>3</sub> perovskite solar cells covering up to 1060 nm. *J. Phys. Chem. Lett.* **2014**, *5*, 1004–1011. [CrossRef]
11. Zuo, F.; Williams, S.T.; Liang, P.-W.; Chueh, C.-C.; Liao, C.-Y.; Jen, A.K. -Y. Binary-metal perovskites toward high-performance planar-heterojunction hybrid solar cells. *Adv. Mater.* **2014**, *26*, 6454–6460. [CrossRef]
12. Liao, W.; Zhao, D.; Yu, Y.; Shrestha, N.; Ghimire, K.; Grice, C.R.; Wang, C.; Xiao, Y.; Cimaroli, A.J.; Ellingson, R.J.; et al. Fabrication of efficient low-bandgap perovskite solar cells by combining formamidinium tin iodide with methylammonium lead iodide. *J. Am. Chem. Soc.* **2016**, *138*, 12360–12363. [CrossRef] [PubMed]
13. Zhao, D.; Yu, Y.; Wang, C.; Liao, W.; Shrestha, N.; Grice, C.R.; Cimaroli, A.J.; Guan, L.; Ellingson, R.J.; Zhu, K.; et al. Low-bandgap mixed tin-lead iodide perovskite absorbers with long carrier lifetimes for all-perovskite tandem solar cells. *Nat. Energy* **2017**, *2*, 17018. [CrossRef]
14. Zhao, D.; Chen, C.; Wang, C.; Junda, M.M.; Song, Z.; Grice, C.R.; Yu, Y.; Li, C.; Subedi, B.; Podraza, N.J.; et al. Efficient two-terminal all-perovskite tandem solar cells enabled by high-quality low-bandgap absorber layers. *Nat. Energy* **2018**, *3*, 1093–1100. [CrossRef]
15. Li, C.; Song, Z.; Zhao, D.; Xiao, C.; Subedi, B.; Shrestha, N.; Junda, M.M.; Wang, C.; Jiang, C.; Al-Jassim, M.; et al. Reducing saturation-current density to realize high-efficiency low-bandgap mixed tin-lead halide perovskite solar cells. *Adv. Energy Mater.* **2018**, *9*, 1803135. [CrossRef]
16. Tong, J.; Song, Z.; Kim, D.H.; Chen, X.; Chen, C.; Palmstrom, A.F.; Ndione, P.F.; Reese, M.O.; Dunfield, S.P.; Reid, O.G.; et al. Carrier lifetimes of >1  $\mu$ s in Sn-Pb perovskites enable efficient all-perovskite tandem solar cells. *Science* **2019**, *364*, 475–479. [CrossRef] [PubMed]
17. Lin, R.; Xiao, K.; Qin, Z.; Han, Q.; Zhang, C.; Wei, M.; Saidaminov, M.I.; Gao, Y.; Xu, J.; Xiao, M.; et al. Monolithic all-perovskite tandem solar cells with 24.8% efficiency exploiting comproportionation to suppress Sn(ii) oxidation in precursor ink. *Nat. Energy* **2019**, *4*, 864–873. [CrossRef]
18. Xiao, K.; Lin, R.; Han, Q.; Hou, Y.; Qin, Z.; Nguyen, H.T.; Wen, J.; Wei, M.; Yeddu, V.; Saidaminov, M.I.; et al. All-perovskite tandem solar cells with 24.2% certified efficiency and area over 1 cm<sup>2</sup> using surface-anchoring zwitterionic antioxidant. *Nat. Energy* **2020**, *5*, 870–880. [CrossRef]
19. Chen, Q.; Luo, J.; He, R.; Lai, H.; Ren, S.; Jiang, Y.; Wan, Z.; Wang, W.; Hao, X.; Wang, Y.; et al. Unveiling roles of tin fluoride additives in high-efficiency low-bandgap mixed tin-lead perovskite solar cells. *Adv. Energy Mater.* **2021**, *11*, 2101045. [CrossRef]
20. Lin, R.; Xu, J.; Wei, M.; Wang, Y.; Qin, Z.; Liu, Z.; Wu, J.; Xiao, K.; Chen, B.; Park, S.M.; et al. All-perovskite tandem solar cells with improved grain surface passivation. *Nature* **2022**, *603*, 73–78. [CrossRef]

21. Li, C.; Song, Z.; Chen, C.; Xiao, C.; Subedi, B.; Harvey, S.P.; Shrestha, N.; Subedi, K.K.; Chen, L.; Liu, D.; et al. Low-bandgap mixed tin-lead iodide perovskites with reduced methylammonium for simultaneous enhancement of solar cell efficiency and stability. *Nat. Energy* **2020**, *5*, 768–776. [[CrossRef](#)]
22. Peng, C.; Li, C.; Zhu, M.; Zhang, C.; Jiang, X.; Yin, H.; He, B.; Li, H.; Li, M.; So, S.K.; et al. Reducing energy disorder for efficient and stable Sn-Pb alloyed perovskite solar cells. *Angew. Chem. Int. Ed.* **2022**, *61*, e202201209. [[CrossRef](#)] [[PubMed](#)]
23. Ghosh, S.; Singh, T. Role of ionic liquids in organic-inorganic metal halide perovskite solar cells efficiency and stability. *Nano Energy* **2019**, *63*, 103828. [[CrossRef](#)]
24. Yoo, D.J.; Kim, A.R.; Balanay, M.P.; Kim, D.H. Alkoxy-substituted triphenylamine based chromophores for dye-sensitized solar cells. *Bull. Korean Chem. Soc.* **2012**, *33*, 33–34. [[CrossRef](#)]
25. Bai, S.; Da, P.; Li, C.; Wang, Z.; Yuan, Z.; Fu, F.; Kawecki, M.; Liu, X.; Sakai, N.; Wang, J.T.-W.; et al. Planar perovskite solar cells with long-term stability using ionic liquid additives. *Nature* **2019**, *571*, 245–250. [[CrossRef](#)]
26. Ambade, S.B.; Ambade, R.B.; Kim, S.; Park, H.; Yoo, D.J.; Leel, S.-H. Performance enhancement in inverted solar cells by interfacial modification of ZnO nanoparticle buffer layer. *J. Nanosci. Nanotechnol.* **2014**, *14*, 8561–8566. [[CrossRef](#)] [[PubMed](#)]
27. Lin, Y.-H.; Sakai, N.; Da, P.; Wu, J.; Sansom, H.C.; Ramadan, A.J.; Mahesh, S.; Liu, J.; Oliver, R.D.J.; Lim, J.; et al. A piperidinium salt stabilizes efficient metal-halide perovskite solar cells. *Science* **2020**, *369*, 96–102. [[CrossRef](#)]
28. Zhang, Y.; Wang, Y.; Zhao, L.; Yang, X.; Hou, C.; Wu, J.; Su, R.; Jia, S.; Shyue, J.; Luo, D.; et al. Depth-dependent defect manipulation in perovskites for high-performance solar cells. *Energy Environ. Sci.* **2021**, *14*, 6526–6535. [[CrossRef](#)]
29. Hu, S.; Otsuka, K.; Murdey, R.; Nakamura, T.; Truong, M.A.; Yamada, T.; Handa, T.; Matsuda, K.; Nakano, K.; Sato, A.; et al. Optimized carrier extraction at interfaces for 23.6% efficient tin-lead perovskite solar cells. *Energy Environ. Sci.* **2022**, *15*, 2096–2107. [[CrossRef](#)]
30. Kapil, G.; Bessho, T.; Sanehira, Y.; Sahamir, S.R.; Chen, M.; Baranwal, A.K.; Liu, D.; Sono, Y.; Hirotani, D.; Nomura, D.; et al. Tin-lead perovskite solar cells fabricated on hole selective monolayers. *ACS Energy Lett.* **2022**, *7*, 966–974. [[CrossRef](#)]
31. Ravichandiran, P.; Prabakaran, D.S.; Maroli, N.; Kim, A.R.; Park, B.-H.; Han, M.-K.; Ramesh, T.; Ponpandian, S.; Yoo, D.J. Mitochondria-targeted acridine-based dual-channel fluorescence chemosensor for detection of Sn<sup>4+</sup> and Cr<sub>2</sub>O<sub>7</sub><sup>2-</sup> ions in water and its application in discriminative detection of cancer cells. *J. Hazard Mater.* **2021**, *419*, 126409. [[CrossRef](#)]